Polymer 51 (2010) 4351–4361

Contents lists available at ScienceDirect

Polymer

journal homepage: www.elsevier.com/locate/polymer

Synthesis, structure characterization and ionic conductivity of star-branched organic–inorganic hybrid electrolytes based on cyanuric chloride, diamine-capped poly(oxyalkylene) and alkoxysilane

Hao-Yiang Wu [a], Diganta Saikia [b], Chi-Pin Lin [b], Feng-Shien Wu [b], George T.K. Fey [c], Hsien-Ming Kao [b,*]

[a] Department of Neurological Surgery, Tri-Service General Hospital, National Defense Medical Center 325, Sec. 2, Cheng-Kung Road, Nei-Hu Dist, Taipei 11490, Taiwan, ROC
[b] Department of Chemistry, National Central University, Chung-Li, Taiwan 32054, Taiwan, ROC
[c] Department of Chemical and Materials Engineering, National Central University, Chung-Li, Taiwan 32054, Taiwan, ROC

ARTICLE INFO

Article history:
Received 15 April 2010
Received in revised form
7 July 2010
Accepted 24 July 2010
Available online 30 July 2010

Keywords:
Organic–inorganic hybrid electrolytes
Cyanuric chloride
Ionic conductivity

ABSTRACT

A synthesis route for preparing highly conductive solid organic–inorganic hybrid electrolytes has been developed by using cyanuric chloride as the coupling core to react with diamino-terminated poly(oxyalkylene) triblock copolymers, followed by cross-linking with an epoxy alkoxysilane 3-glycidyloxypropyl trimethoxysilane via a sol-gel process. The present hybrid electrolyte with a [O]/[Li] ratio of 32 was found to be the most conductive, reaching a maximum lithium ion conductivity of 6.8×10^{-5} Scm^{-1} at 30 °C. The Li-ion mobility was determined from ^{7}Li static NMR line width measurements and correlated with their ionic conductivities. The onset of ^{7}Li line narrowing was closely related to the T_g of the hybrid electrolytes as measured by DSC experiments. Thus, the motions of the lithium cations are strongly coupled with the segmental motion of the polymer chains, which is in line with the Vogel-Tamman-Fulcher behavior as observed in ionic conductivity.

1. Introduction

Designing new ion-conducting polymer materials has been the subject of intense research due to its promising applications in the fields of Li-ion batteries, supercapacitors, dye-sensitized solar cell, and electrochromic devices [1–5]. The use of polymers in developing electrolyte materials combines the ease of processability, design flexibility, lightweight, shape versatility, safety and lack of toxicity. As Li-ion batteries are considered to be one of the most reliable future energy storage systems, which can provide power ranges from modern electronic devices like cellphone and laptops to electric or hybrid electric vehicles (EV or HEVs), the use of polymer electrolytes in Li-ion batteries offers great promise for the development of low cost, long life and safe lithium-based battery technologies. Solid polymer electrolytes (SPEs) are considered as alternatives to liquid and gel electrolytes because of leakage proof and good mechanical properties. In addition, it is possible to avoid the hazardous chemicals which are used as solvents in liquid and gel polymer electrolytes.

The main concern of SPEs is their low ionic conductivity. The ionic conductivity of SPEs is due to the motion of dissolved ionic species (cations and anions) in a polymeric matrix and in most cases occurs in the amorphous phase, above the glass transition temperature, T_g, via a liquid like motion of the cations associated with segmental reorientations of the neighboring chains [6]. Although poly(ethylene oxide) (PEO) has been intensively studied as a host matrix to dissolve lithium salts because it contains ether coordination sites and flexible polymer structures, the major disadvantage associated with PEO-based polymer electrolytes is their ionic conductivity at ambient temperature ($\sim 10^{-7}$ Scm^{-1}). This is due to the existence of crystalline domains that interfere with the ion transport and the dependence of the ion transport on the main-chain segmental motions [7]. To overcome this disadvantage, considerable research efforts have been adopted to increase the volume fraction of the amorphous domain in the polymer host by using polymers with low T_g, addition of inorganic sub-micron and nano-sized fillers, synthesis of organic–inorganic hybrid materials, and so on [8–14]. Among these, the organic–inorganic hybrid electrolytes are of particular interest because of their highly flexible structures with enhanced segmental mobility as well as high thermal stability. Another advantage is the ease of modifying their properties by a broad choice of different side groups attached to the silicon atoms.

In the present work, we investigated the dynamic properties of hyperbranched copolymers made from inorganic siloxane and polyalkylene oxide units connected by using 2,4,6-trichloro-1,3,5-triazine (cyanuric chloride) as the central core linking unit.

* Corresponding author. Fax: +886 3 4227664.
E-mail address: hmkao@cc.ncu.edu.tw (H.-M. Kao).

0032-3861/$ – see front matter © 2010 Elsevier Ltd. All rights reserved.
doi:10.1016/j.polymer.2010.07.039

Cyanuric chloride is chosen as the linking unit because it can provide three branching sites to sequentially react with a series of amine-terminated alkylene oxides at different temperatures. With this reaction strategy, a star polymer was made by reacting three of the aryl chlorides with the diamino-alkylene oxide (Scheme 1), followed by the reaction with 3-glycidoxypropyl trimethoxysilane (GLYMO). GLYMO provides a cross-linking unit through a sol-gel process to increase the mechanical strength of the resulting free-standing film. A systematic study was performed, in which oxygen-to-lithium ratio and molecular weight of the polymer were varied in order to understand these variables on the ionic conductivity and other properties of the resulting polymer films. Multinuclear (^{13}C, ^{29}Si, ^{7}Li) solid-state NMR techniques were implemented in order to gain more insights into the role of ion-polymer interactions, the nature of the charge carriers, and the ionic association process in the ionic conductivity. Furthermore, Fourier transform infrared (FTIR), differential scanning calorimetry (DSC), ionic conductivity, lithium transference number and linear sweep voltammetry measurements were carried out for elucidation of the influence of the material compositions on their properties.

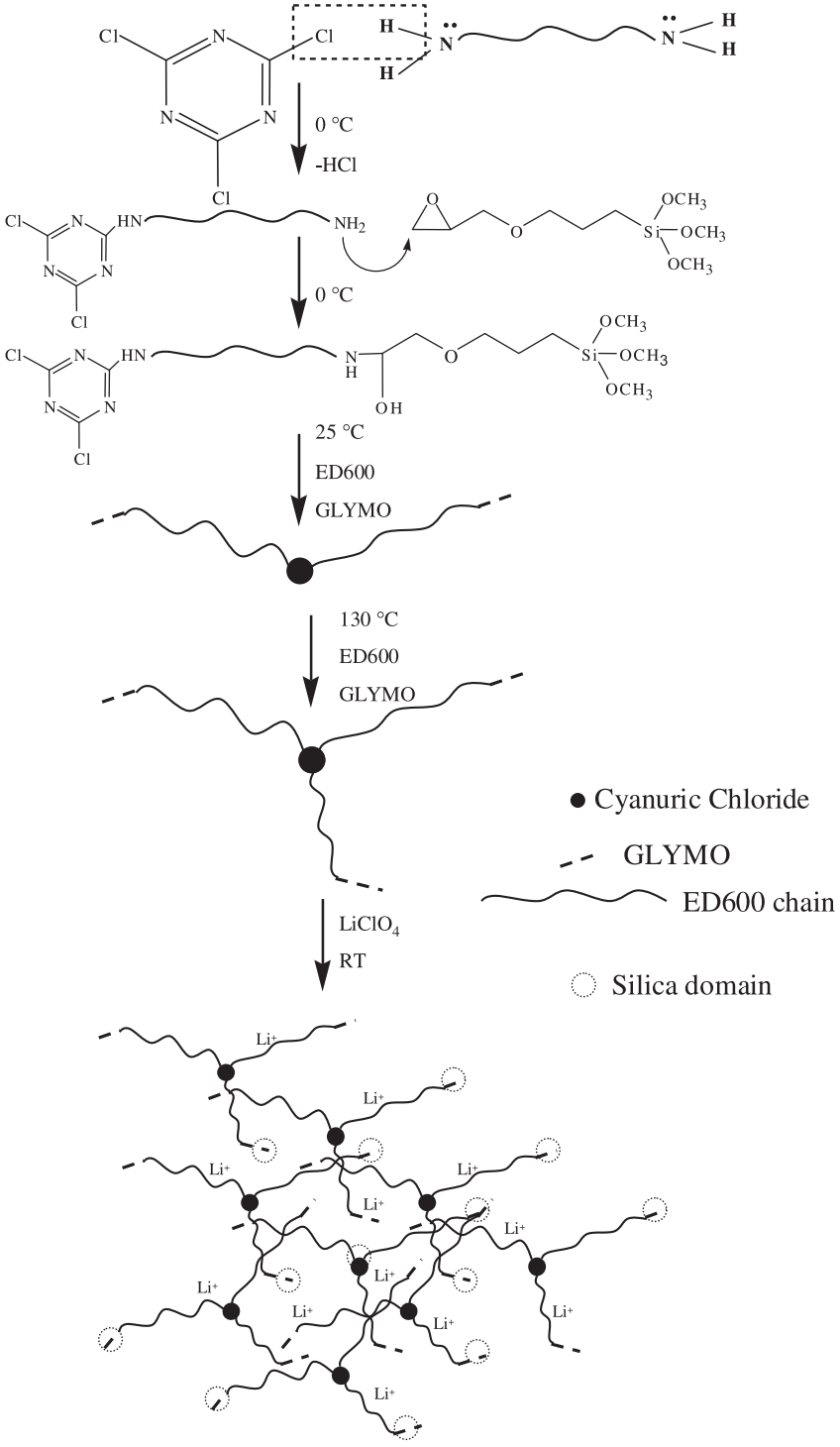

Scheme 1. Schematic representation of the structure of the present hybrid electrolyte.

2. Experimental section

2.1. Materials

Lithium perchlorate ($LiClO_4$, Aldrich) and poly(propylene glycol)-*block*-poly(ethylene glycol)-*block*-poly(propylene glycol) bis(2-aminopropyl ether) (H_2N-PPG-PEG-PPG-NH_2, Aldrich, commercially designated by Jeffamine ED-2000, ED-900, and ED-600 with $M_w = 2000$, 900, and 600 g/mol containing about 40.5, 15.5, and 8.5 PEG units, respectively) were dried under vacuum for two days prior to use. Both cyanuric chloride (denoted as CC) and GLYMO were purchased from Aldrich and used as received. Tetrahydrofuran (THF) was distilled from sodium/benzophenone prior to use.

2.2. Synthesis of hybrid electrolyte films

Scheme 1 illustrates the synthesis process and the structure of $LiClO_4$-doped hybrid electrolytes. In a typical synthesis process, equimolar amounts of ED-x ($x = 600$, 900 or 2000) and cyanuric chloride were dissolved in 5 mL and 50 mL of THF, respectively. The reaction temperature of both solutions was lowered to 0 °C in ice bath. The cyanuric chloride solution was then added to the diamine-capped polyalkylene oxide solution and stirred for 2 h at 0 °C. These diamines contain a mixture of ethylene oxide and propylene oxide units in the chain. The ethylene oxide promotes lithium ion conductivity while the propylene oxide units help to suppress crystallization [15]. With this solution, GLYMO was added and stirred for 6 h at 0 °C. The reaction temperature was slowly increased to room temperature (25 °C) and ED-x was added followed by stirring for 24 h. Then GLYMO was added into the above solution and stirred for another 24 h. No gel formation was observed during the reaction, which gave evidence that the polymer was not cross-linking prematurely via reaction of the third reactive site on cyanuric chloride. Each stage of the product was verified with ^{13}C solution NMR by monitoring the changes in the carbon atoms of the CC ring and the appearance of the ether carbon of ED-x and the alkyl chain of GLYMO added. Once the linear polymer was made, the third site was reacted at 130 °C to provide cross-linked networks. In order to do that, ED-x was added to the solution at 130 °C and refluxed for 24 h. After addition of GLYMO, the above solution was stirred for another 24 h. Finally, the solution was cool down to room temperature and the salt $LiClO_4$ corresponding to various [O]/[Li] ratios was dissolved in the solution and stirred at room temperature for 24 h. The resulting viscous solution was then cast onto Teflon dishes and air dried for 2 days to remove solvent. The films were further cured at 60 °C for 2 days. After vacuum dried at 80 °C for 2 days, the final polymer electrolyte films were obtained. The resulting films were immediately transferred into a glove box (VAC, MO 40-1) under argon atmosphere to avoid any absorption of moisture. The thickness of the films was controlled to be in the range of 150–200 μm. The cross-linked polymer electrolyte films were strong and highly elastic in nature. The resulting hybrid electrolytes were designated as C(X)–Z, where C stands for the cross-linking polymer synthesized by reaction with diamine-capped polyalkylene oxide oligomers, cyanuric chloride and GLYMO, X corresponds to the average molecular weight of the starting polymer, either 2000, 900 or 600, and Z (salt composition) indicates the number of ether oxygen atoms (only for polymer) per Li^+ cation.

2.3. Characterization methods

Differential scanning calorimetry (DSC) was performed in the temperature range from −60 to 125 °C using Perkin–Elmer Pyris 6 DSC at a heating rate of 5 °C/min calibrated with indium and hexyl bromide. The sample weights were maintained in the range of 7–10 mg and were hermetically sealed in aluminum pans. The T_g values were then determined using the fictive temperature method in the Pyris software. The reported DSC curves were the second heating scans taken after an initial heating scan to erase the thermal history, followed by quenching to −60 °C. The enthalpy of melting (ΔH_m) was determined by the integration of the peak area under a linear baseline.

FTIR spectra were obtained from a Bio-Rad FTS155 spectrometer at a resolution of 4 cm^{-1} using the KBr wafer technique. Band deconvolution of the resulting spectra was conducted to obtain the best fit for the band envelope in the spectral range of 600–650 cm^{-1}.

Alternating current (AC) impedance measurements of the hybrid electrolytes were performed using Autolab/PGSTAT 302 frequency response analyzer over a frequency range of 10 Hz–1 MHz with an amplitude of 10 mV. All the specimens were sandwiched by two polished stainless steel blocking electrodes for conductivity tests. These measurements were performed in the temperature range of 5–90 °C, and the system was thermally equilibrated at each selected temperature for at least 1 h. Complex impedance plots (semi-circles) were computed from the raw experimental data. The intersection in the imaginary impedance at low frequency with the real impedance axis corresponds to the ionic conductance of the samples and hence the conductivity values (σ) are obtained from the equation $\sigma = (1/R_b)(t/A)$, where R_b represents the bulk resistance, t is the thickness and A is the area of the sample.

The lithium transference number (t_+) was determined by using a combination method of dc polarization and ac impedance measurements, which has been reported by Evans et al. [16] with the equation shown as follows,

$$t_+ = \frac{I_s(\Delta V - I_0 R_0)}{I_0(\Delta V - I_s R_s)} \quad (1)$$

where ΔV is the potential applied across the cell. I_0 and I_s are the initial and steady-state dc currents, and R_0 and R_s are the initial and steady-state resistances of the passivating layers. The current and resistance were measured from an Autolab/PGSTAT 302 impedance analyzer. The sample was sandwiched between two 0.5 mm-thick lithium foils (Alfa) as non-blocking electrodes and assembled in a standard 2032 coin-cell holder in an argon gas-filled glove box. Finally, it was placed into an outside oven, which was held the temperature at 75 °C. The dc voltage pulse applied to the cell was 10 mV.

The electrochemical stability of the hybrid electrolytes was determined by linear sweep voltammetry (LSV) using stainless steel (SS) as a working electrode and lithium as counter and reference electrodes for a Li/C(X)–Z hybrid electrolyte/SS cell at a scan rate of 1 mVs^{-1} from 0 to 8 V vs. Li/Li^+.

Solid-state NMR experiments were performed on a Varian Infinityplus-500 NMR spectrometer, equipped with a Chemagnetics 7.5 mm MAS probe and a static double resonance probe. The Larmor frequencies for ^7Li, ^{13}C, and ^{29}Si nuclei were 194.3, 125.7, and 99.3 MHz, respectively. ^{13}C, ^{29}Si, and some ^7Li NMR spectra were acquired under conditions of magic angle spinning (MAS) with a spinning speed in the range of 3–5 kHz. The Hartmann–Hahn condition for ^1H to ^{13}C cross-polarization (CP) experiments was set up by using admantane as a standard compound. The ^{13}C CPMAS (cross-polarization magic angle spinning) NMR signal intensities were also recorded as a function of CP contact time ranging from 0.2 to 10 ms. The $\pi/2$ pulse lengths for ^7Li and ^{29}Si nuclei were typically 4 and 6 μs, respectively. The ^{13}C and

^{29}Si chemical shifts were externally quoted to tetramethylsilane (TMS) at 0 ppm. ^{7}Li NMR spectra were acquired under static and MAS conditions with and without proton decoupling during the acquisition. The ^{7}Li line widths from the static measurements were taken to be the full-width at half-height (FWHH) of the peaks and measured as a function of temperature from −100 to 100 °C.

^{1}H wide-line NMR spectra were acquired with the use of the 2D WISE (WIdeline SEparation spectroscopy) NMR pulse sequence developed by Schmidt-Rohr et al. [17]. In the 2D WISE NMR experiments, the proton magnetization evolved under the influence of dipolar coupling during the time t_1 and the ^{13}C signal was detected under MAS conditions during the time t_2. The experiment revealed proton wide-line spectra from the proton of the polymer chains along the ω_1 dimension, resolved by the ^{13}C chemical shifts of polymer chains along the ω_2 dimension. Therefore, a correlation can be made between the chemical structure and segmental mobility of the polymer. Spectral widths of 40 and 100 kHz were used for the ω_2 and ω_1 dimensions, respectively. Typically 100 t_1 increments were used in the 2D WISE NMR experiments.

3. Results and discussion

3.1. Thermal behaviors

Typical DSC traces for the C(600)–Z and C(2000)–Z hybrid electrolytes with and without doping the lithium salt are shown in Fig. 1. When the salt concentration was increased, the T_g of the hybrid electrolytes increased markedly. Table 1 displays the T_g values of C(X)–Z electrolyte systems with various [O]/[Li] ratios.

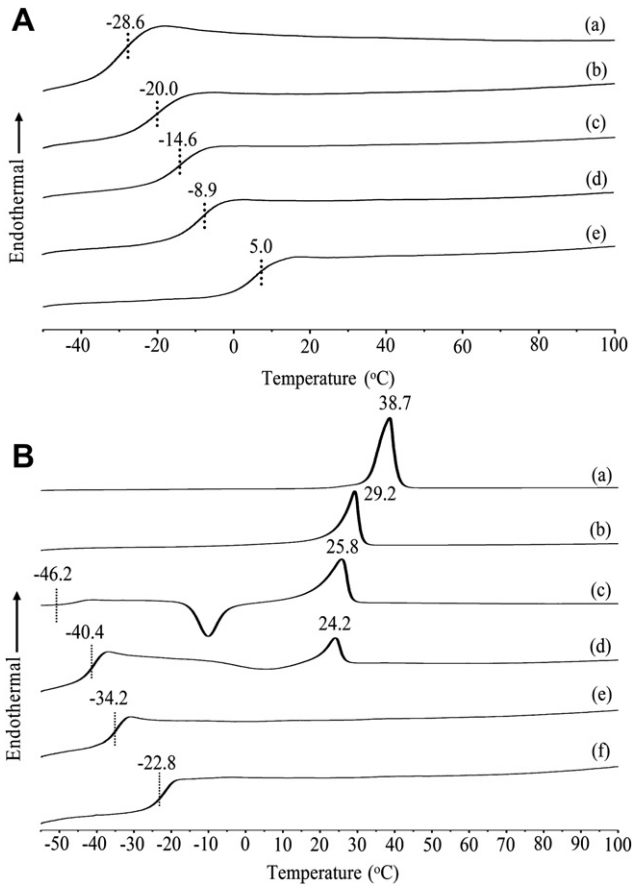

Fig. 1. DSC thermograms of (A) C(600)–Z hybrids with various [O]/[Li] ratios, Z = (a) ∞, (b) 32, (c) 24, (d) 16, (e) 8 and (B) C(2000)–Z hybrids with (a) Pure ED-2000, Z = (b) ∞, (c) 32, (d) 24, (e) 16, and (f) 8. The T_g value was indicated by the dashed line.

Table 1
DSC results of the hybrid electrolytes studied.

Z, [O]/[Li]	C(600)	C(900)	C(2000)		
	T_g, °C	T_g, °C	T_g, °C	T_m, °C	χ(%)[a]
∞	−28.6	–	–	29.2	70.0
32	−20.0	−34.8	−46.2	25.8	46.0
24	−14.6	−28.6	−40.4	24.2	3.1
16	−8.9	−23.7	−34.2	–	–
8	5.0	−4.0	−22.8	–	–

[a] Considering the degree of crystallinity (χ) of pure ED-2000 is 100% .

The increase in T_g can be attributed to ion–dipole interactions that reduce the segmental motion of the hybrid electrolytes. This behavior is similar to most of polymer electrolytes formed by complexation of a Li-salt with a polyether-based polymer, in which glass transition temperature tends to increase with an increase in the salt concentration. The thermogram of C(2000)–32 (part c in Fig. 1B) exhibited an exothermic peak around −10 °C, corresponding to the recrystallization of ED-2000 [18]. The exothermic peak disappeared when the salt concentration was further increased. This implied that the recrystallization process was affected by the amount of salts presented in the hybrid materials.

Another hybrid electrolyte series C(900)–Z (Fig. S1, Supplementary content, SC) are in the amorphous state because no melting transition is observed in the thermograms. Although C(2000)–Z series shows melting temperature (T_m) and the endothermic heat (ΔH_f), these parameters are decreased and disappeared with increasing salt concentrations. It indicates that the crystalline structure of C(2000) is disrupted and is gradually transformed into an amorphous form with the addition of $LiClO_4$.

3.2. FTIR analysis

FTIR was employed to provide the information about the development of the organic–inorganic network and to study the interaction of the polymer backbones with the lithium salts. Fig. 2 shows the FTIR spectra of pure ED-2000 and C(2000)–Z hybrid electrolyte with various [O]/[Li] ratios. One major peak associated with C–O–C asymmetric stretching vibration was observed at 1110 cm^{-1} for pure ED-2000 (Fig. 2a). While GLYMO was incorporated into the polymer matrix, the peak became broader since the characteristic absorption bands of GLYMO were also expected to appear in the same region (Fig. 2b–f). A medium intensity band at 950 cm^{-1} was assigned to the coupled vibration of C–C stretching and CH_2 rocking modes [19]. There is a possibility of the absorption band due to Si–OH in the hybrid materials which overlaps with the band frequency at 950 cm^{-1} [20]. The presence of Si–OH groups can be further confirmed by ^{29}Si NMR studies as shown below. With the addition of lithium salt, two sharp peaks at 1120 and 1110 cm^{-1} appeared, suggesting that the ether group of ED-2000 had some interactions with the lithium cations added. Although the changes in the intensity, shape, and position of the C–O–C stretching mode are associated with the polyether–$LiClO_4$ interactions, the dependence of the absorption peaks of C–O–C on the salt concentrations is not easily clarified in the FTIR spectra since the absorption peaks of C–O–C seriously overlap with those of Si–O–Si and Si–O–C. The peaks at 2880 and 1650 cm^{-1} were assigned to CH_2 symmetric stretching and NH stretching, respectively. The medium intensity band observed at 1562 cm^{-1} is attributed to the amide II mode [21]. The amide II band consists of the vibration of the N–H in-plane bending, the C–N stretching, and the C–C stretching modes [21–23]. Other absorption peaks at 1460, 1351, 1300, 1260 and 844 cm^{-1} were due to CH_2 bending, wagging, twisting and rocking vibrations, respectively.

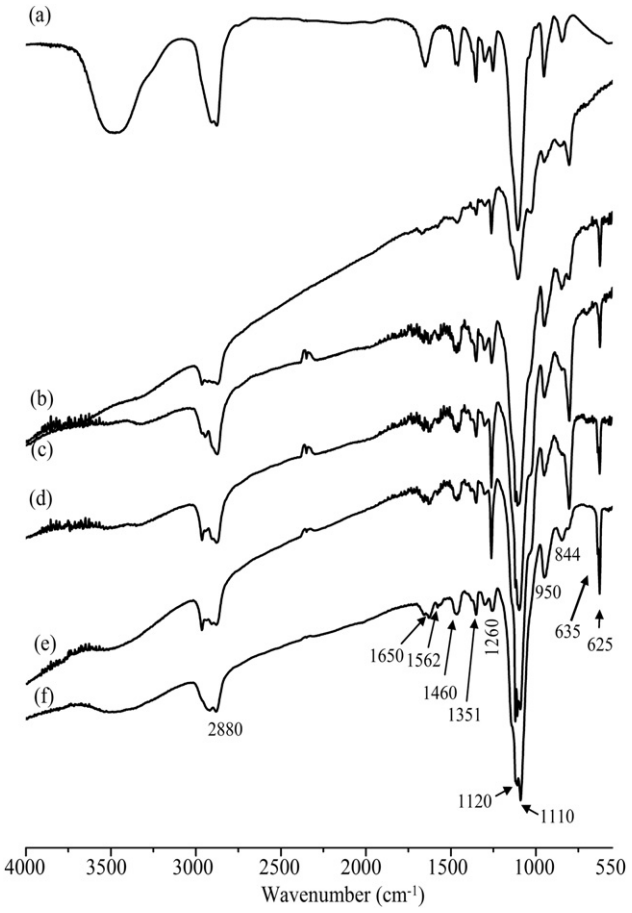

Fig. 2. FTIR spectra of (a) pure ED-2000 and C(2000)–Z hybrids with various [O]/[Li] ratios, Z = (b) ∞ (c) 32, (d) 24, (e) 16, and (f) 8.

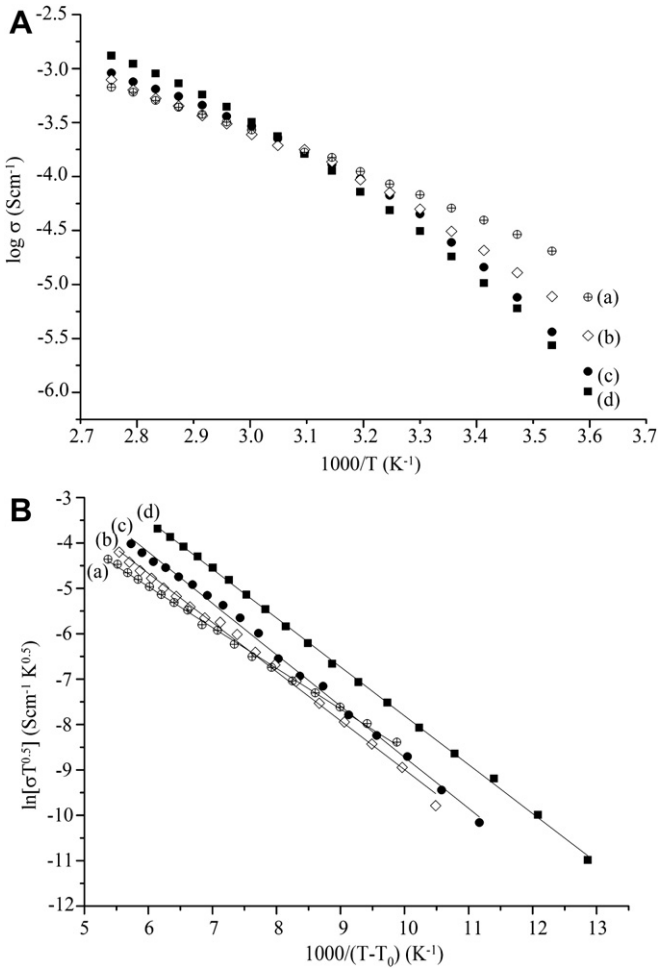

Fig. 3. Temperature dependence of ionic conductivity (A) and its VTF fitting curves (B) of C(2000)–Z hybrids with various [O]/[Li] ratios, Z = (a) 32, (b) 24, (c) 16 and (d) 8.

The vibrational modes of the ClO_4^- anion in the range of 600–650 cm^{-1} can be used as effective probes to estimate the extent of ionic association. Two bands were observed at 625 and 635 cm^{-1} due to the vibration modes of the ClO_4^- anions [24–26]. The band centered at 625 cm^{-1} has been assigned to the vibration of the "free" ClO_4^- anion, which does not interact directly with the lithium cations, whereas the band centered at 635 cm^{-1} is ascribed to the vibration of the $Li^+ClO_4^-$ contact-ion pairs. The spectral features of the $\nu(ClO_4^-)$ modes are fitted with Gaussian–Lorentzian functions to investigate the behavior of ionic association in the present hybrid system and the deconvoluted curves of C(2000)–Z hybrids are shown in Fig. S2 (SC). The fractions of free anions as a function of salt concentrations for the C(*X*)–Z hybrid electrolytes are listed in Table 2. These fractions are calculated as the ratio of the area under the 625 cm^{-1} mode to the total area under the $\nu(ClO_4^-)$ envelope. As seen in Table 2, the fraction of free anions decreases with increasing salt concentrations. About 89–95% of ClO_4^- exists as spectroscopically free species for the hybrid electrolyte with a [O]/[Li] ratio of 32, while only about 64–68% is observed for the [O]/[Li] ratio of 8 in the electrolyte series. Thus, a higher percentage of free anions for a [O]/[Li] ratio of 32, helps the lithium cations to move more freely, and thus results in a higher ionic conductivity compared to other [O]/[Li] ratios.

3.3. Ionic conductivity

Fig. 3 shows the temperature dependence of the conductivity for C(2000) based hybrid electrolytes with various [O]/[Li] ratios. The variation of conductivity with temperatures suggests a Vogel-Tamman-Fulcher (VTF) behavior as is often observed for amorphous polymer electrolytes, indicating that the ion mobility is coupled with the segmental motion of the polymer chain. The C(2000)–Z electrolyte, with a [O]/[Li] ratio of 32, exhibited the

Table 2
Conductivity (at 30 °C), transference number and FTIR deconvolution results of the hybrid electrolytes studied.

Z, [O]/[Li]	C(600)		C(900)		C(2000)		
	σ (Scm^{-1})	free ClO_4^-, %	σ (Scm^{-1})	free ClO_4^-, %	σ (Scm^{-1})	free ClO_4^-, %	Transference number, t_+
32	3.74×10^{-6}	95	2.02×10^{-5}	89	6.80×10^{-5}	92	0.26
24	1.72×10^{-6}	88	1.31×10^{-5}	83	4.99×10^{-5}	84	0.28
16	1.66×10^{-6}	80	6.84×10^{-6}	73	4.49×10^{-5}	70	0.29
8	1.09×10^{-6}	68	5.13×10^{-6}	65	3.12×10^{-5}	64	0.31

highest ionic conductivity value of 6.8 × 10^{-5} Scm^{-1} at 30 °C. Further increase in the salt contents results in a remarkable decrease in the total ionic conductivity. To study the influence of host dynamics on ion transport, the ionic conductivities of C(600)–Z and C(900)–Z hybrid electrolytes with various salt concentrations were also measured (Figs. S3 and S4, SC) and maximum ionic conductivity values of 3.7 × 10^{-6} and 2 × 10^{-5} Scm^{-1} were obtained, respectively. The conductivity values for the hybrid electrolytes films as a function of salt concentration are summarized in Table 2. It is observed that the ionic conductivity is maximum for C(2000)–Z and gradually decreases for C(900)–Z and C(600)–Z hybrid electrolyte systems. This may be attributed to the longer PEG chains of ED-2000, compared to those of ED-900 and ED-600. The longer PEG chains may increase the proportion of the amorphous phase in the electrolyte samples. In addition, the low T_g value of C(2000)-Z in comparison to C(900)-Z and C(600)-Z increases the flexibility and chain mobility of the polymer, which is beneficial to the enhancement of the ionic conductivity. Moreover, the higher percentage of PEG to PPG ratio in ED-2000 than ED-900 and ED-600 (about 40.5, 15.5, and 8.5 PEG units contain in ED-2000, ED-900 and ED-600, respectively) helps in the enhancement of conductivity as PPG is known to be a poor conductor of ions [15]. The higher amount of PEG units in ED-2000 creates higher number of PEG branching sites. These branching sites improve the free movement of polymer chain and hence lower the T_g [15]. Therefore, the highest ionic conductivity is observed in the C(2000)–Z system.

The ionic conductivity of PEO-based solid polymer electrolyte is around 10^{-7} Scm^{-1} at ambient temperature. For solid (solvent-free) polymer electrolytes, the highest conductivity value is still around 10^{-4} Scm^{-1}. In particular, the conductivity value for organic–inorganic hybrid electrolytes (solvent free) is relatively low, for example, around 10^{-5}–10^{-6} Scm^{-1}. Depending on the connection between the organic (polymer) and inorganic (siloxane) phases, two types of organic–inorganic hybrid electrolytes have been reported [27–29]. In the type I materials, organic and inorganic components are linked through weak physical bonds such as hydrogen bridges or van der Waals bonds. In the type II hybrids, on the other hand, organic and inorganic phases are connected with covalent bonds. Although the type I hybrids have higher room temperature ionic conductivities (up to 10^{-4} Scm^{-1}) than the type II hybrids, the type I hybrids often have much lower chemical stabilities. The present hybrid belongs to the type II hybrid with an ionic conductivity value up to 6.8 × 10^{-5} Scm^{-1} at 30 °C, which is higher as compared to most of the organic–inorganic hybrids reported in the literature [30–34]. Besides, the room-temperature conductivity value of the present hybrid electrolytes is at least two orders of magnitude higher than that of the PEO-based electrolytes and is also comparable to the highest conductivity values reported for most of the polymer electrolytes with various modifications [35–38]. The ionic conductivity of the C(2000)-8 reaches 3 × 10^{-3} Scm^{-1} at 30 °C after plasticization with ethylene carbonate (EC)/propylene carbonate (PC) (1:1, v/v) and thus is promising for further electrical applications.

Table 3
VTF parameters for the hybrid electrolytes studied.

Z	C(600)			C(900)			C(2000)		
	T_0 (K)	A (Scm^{-1} $K^{1/2}$)	B (kJ/mol)	T_0 (K)	A (Scm^{-1} $K^{1/2}$)	B (kJ/mol)	T_0 (K)	A (Scm^{-1} $K^{1/2}$)	B (kJ/mol)
32	203	0.13	6.21	188	1.38	7.60	176	1.54	7.48
24	208	1.18	8.20	194	2.53	8.38	182	6.14	8.99
16	214	0.97	7.60	199	5.89	9.24	188	16.84	9.72
8	228	0.51	6.20	218	2.32	7.00	200	19.4	8.96

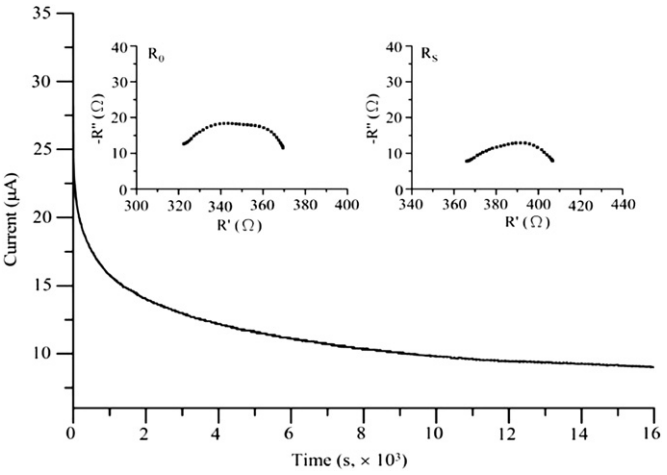

Fig. 4. Typical depolarization curve of C(2000)–24 hybrid polymer electrolyte.

The conductivity data were fitted according to the VTF equation,

$$\sigma(T) = AT^{-1/2}\exp\left(\frac{-B}{T-T_0}\right) \quad (2)$$

where A is the pre-exponential factor, which is related to the charge carrier concentration in the polymer electrolyte, B is the

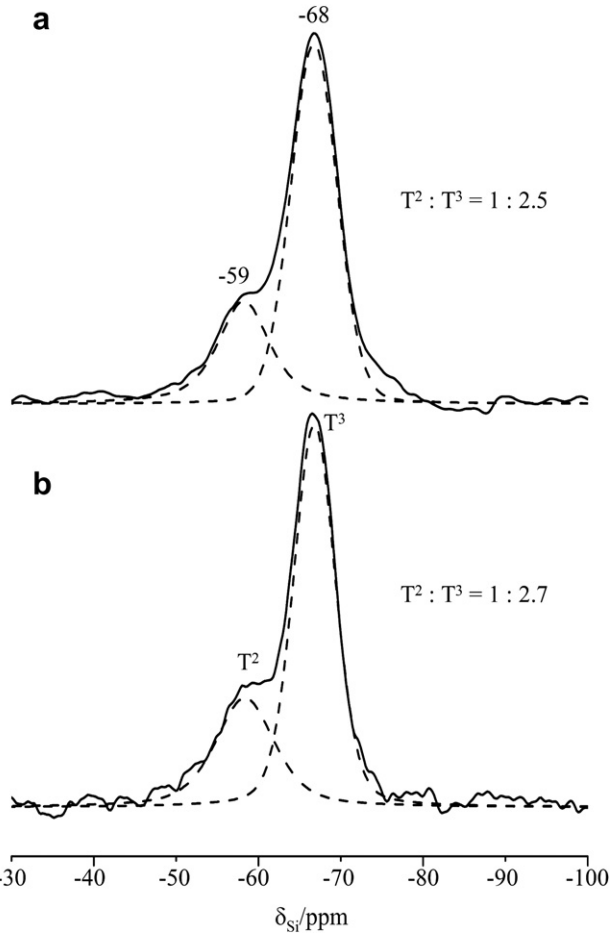

Fig. 5. ^{29}Si MAS NMR spectra of C(600)–Z hybrids with [O]/[Li] ratios, Z = (a) 32 and (b) 8. The dashed lines represent the components used for the spectral deconvolution.

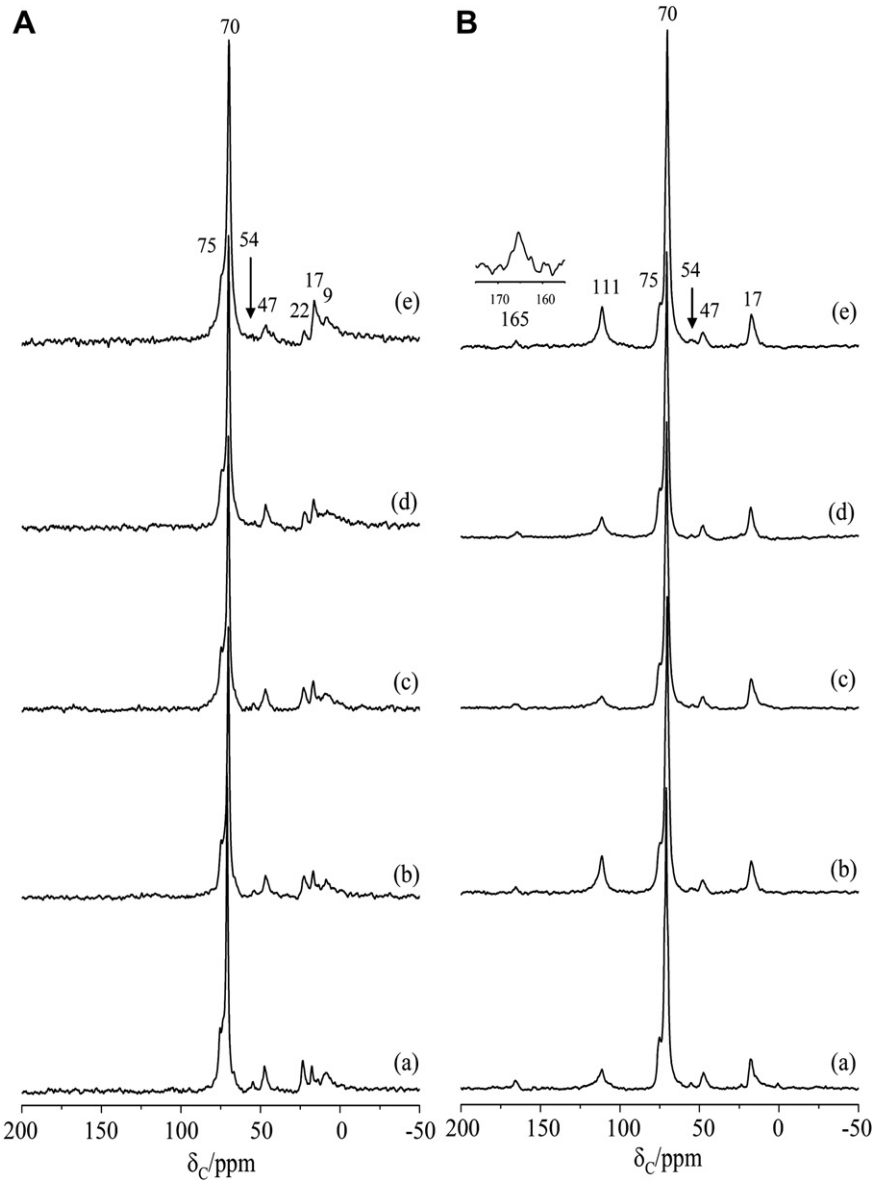

Fig. 6. ^{13}C CPMAS (A) and MAS (one-pulse) (B) NMR spectra of C(600)–Z hybrids with various [O]/[Li] ratios, Z = (a) ∞, (b) 32, (c) 24, (d) 16, and (e) 8.

pseudo-activation energy of the ion transport related to the configurational entropy of the polymer chains, T_0 is the ideal transition temperature at which relaxation times become infinite and the free volume disappears, and R is the perfect gas constant, 8.314 J K^{-1} mol^{-1}. According to the literature reported on polyether-based polymer electrolytes, in which T_0 was found to be approximately $T_g - 50$ [39], T_0 was fixed at $T_g - 50$ K for the present electrolytes and a good fit to the data was achieved. The VTF equation predicts that a plot of $\ln(\sigma T^{1/2})$ vs. $1/(T-T_0)$ should be linear, which is exactly observed in Fig. 3B. The values of the VTF parameters for the hybrid electrolytes are listed in Table 3. The A parameter in equation (2) tends to increase as the salt concentration is increased. Moreover, the calculated values of the pseudo-activation energies, B, increase with the salt concentration as well as T_0 and T_g. The values of B are almost similar to the previously reported works and show almost the same type of trend [40–43]. The decrease in A and B values at higher salt concentrations, especially for C(900) and C(600), may be due to the aggregation of salt which reduces the ion transport.

The conductivity was governed by several factors including the cation and anion types, salt concentration, temperature, etc. To obtain a highly conductive SPE, two factors on the ionic transport properties must be thoroughly understood, namely the numbers and mobility of the charge carriers on the basis of the following equation.

$$\sigma(T) = \sum_i n_i q_i \mu_i \tag{3}$$

where n_i is the number of charge carriers, q_i is the charge on each charge carrier, and μ_i is the mobility of charge carriers. According to equation (3), the ionic conductivity depends on the amount of charge carriers in the system and the mobility of the various species. As the ion transport mechanism in solvent-free polymer electrolytes is dependant on the local motion of polymer segments [44], the components which increase free volume may be expected to have a beneficial influence on conductivity. The non-linearity of temperature dependence of ionic conductivity indicates that ion

transport in polymer electrolytes is dependent on polymer segmental motion. As the salt concentration is increased, the number of charge carriers is increased according to the FTIR results. Nevertheless, the average free volume is decreased as indicated from the increase in T_g owing to the interaction of Li^+ with ether oxygens. The solvation of the lithium cation by the PEG and PPG segments partially interrupts the local motion of the polymer segment via the formation of transient cross-links, as indicated by the increase in T_g with increasing salt concentrations. At a relatively high $LiClO_4$ concentration (e.g., [O]/[Li] = 8), the formation of ion pairs or aggregates decreases the number of free charge carriers present. These aggregates are anticipated to contribute less effectively to ion transport and somehow hinder the mobility of the free charge carriers throughout the polymer matrix. Moreover, the formation of transient ion-polymer cross-links would be expected to restrict segmental mobility and therefore reduce conductivity. Both effects result in a reduction in bulk ionic conductivity at high salt concentrations. At low salt concentration levels, on the other hand, the decrease in the free volume is not significant and the extent of contact-ion pairs is low as well. As a result, the conductivity is dominated by the mobility of charge carriers. Although the number of charged mobile species is less at higher values of *Z*, the dissociation of the salt to form charged species is greater, at least partially compensating for the effects of lower salt concentrations.

3.4. Lithium transference number

As the C(2000)–Z hybrid system showed maximum ionic conductivity in comparison to C(900)–Z and C(600)–Z series, its transference number measurement was carried out in C(2000)–Z series. The typical depolarization curve of C(2000)–Z hybrid electrolyte is shown in Fig. 4 and the corresponding values of lithium ion transference number are given in Table 2. It is observed that the transference number increases with [O]/[Li] ratios. This increase in t_+ can be attributed in two ways. We have found from the conductivity results that although room temperature conductivity of C(2000)-Z hybrid electrolyte with [O]/[Li] = 32 is higher and decreases towards [O]/[Li] = 8, but the conductivity at 75 °C follows the reverse order, i.e., conductivity of [O]/[Li] = 8 is higher and decreases towards [O]/[Li] = 32. At elevated temperature (75 °C) lithium ions get more free space to move and with increase in salt concentration more lithium ions get free and hence t_+ increases with decreasing [O]/[Li] ratios. Although the FTIR deconvoluted data (Table 2) indicate that the proportion of free perchlorate decreases with increasing salt concentrations, the total amount of lithium ions increases more (by 4 times) than the decrease in the free perchlorate amount (decrease by ~1/3). This suggests that the actual amount of free lithium ions should be more than the value obtained from FTIR, which increases with salt concentrations. As a result, t_+ increases with the increase in the lithium salt content. Another factor which governs the changes in t_+ values is anion mobility. The increase in t_+ values with increase in salt concentration may also be ascribed to the decrease in mobility of the anions due to a decrease in free volume with increasing density [45].

3.5. ^{29}Si MAS NMR

To determine the structure of the silicate networks developed in the present hybrid materials, solid-state ^{29}Si NMR measurements were performed. Fig. 5 displays the deconvoluted ^{29}Si MAS NMR spectra of C(600)–Z with [O]/[Li] ratios of 32 and 8. The peaks around −67 and −58 ppm, corresponding to T^3 ($RSi(OSi)_3$, R represents an alkyl group) and T^2 ($RSi(OSi)_2(OH)$) sites were observed for both the selected [O/Li] ratios. The observation of T groups indicated the presence of organosilane groups in the materials. This organosilane was stable under synthesis conditions since the Si–C cleavage for the formation of Q ($Si(OSi)_4$) groups was not observed. The spectral features were basically the same for both samples, and the populations of various silicon environments (T^2 vs. T^3) showed minor changes as a function of salt concentrations, reflecting that the presence of $LiClO_4$ had no significant influence on the hydrolysis and condensation process of GLYMO.

3.6. Solid-state ^{13}C NMR

Solid-state ^{13}C NMR experiments were performed to probe the backbone structure of the hybrid electrolytes. Fig. 6 shows the ^{13}C CPMAS and MAS (one-pulse) NMR spectra of C(600)–Z hybrids with various [O]/[Li] ratios. The most predominant peak at 71 ppm can be assigned to the methylene carbons in the alkylene oxide units in the diamine portions of ED-600. The methyl carbon from the propylene oxide units appear at 18 ppm, while the peak at 46 ppm can be assigned to the nitrogen substituted carbons at the terminal of the diamines. The weak signal at 165 ppm due to the –C=N– in the central core CC was observed by direct polarization in the one-pulse experiment. The peaks at 23 and 10 ppm are assigned to the methylene carbons in the α and β positions to the silicon atom, respectively, due to GLYMO [21]. The ^{13}C peak at 54 ppm is observed due to the carbon atoms in the epoxide ring of GLYMO, indicative of the incompleteness of the epoxide ring opening. The peak at 75 ppm results from the $-OCH_2$ groups of the

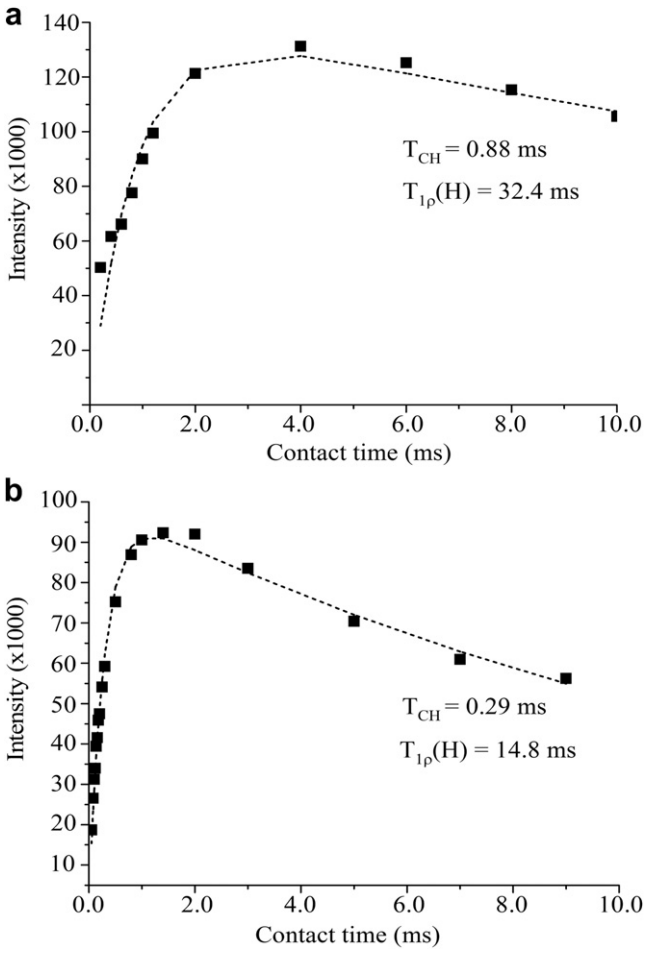

Fig. 7. ^{13}C CPMAS signal at 71 ppm of C(600)–Z hybrids, where Z = (a) 32 and (b) 8, as a function of contact time.

PEG and PPG segments at chain ends. The NMR observations are consistent with the hybrid structure as illustrated in Scheme 1.

Due to complex environments in the region of 72–75 ppm, we focused on the ^{13}C CP signal intensity for the ether carbon at 71 ppm as a function of contact time and salt doping levels. The results of the contact time measurements for the peak at 71 ppm of C(600)–Z hybrids with various [O]/[Li] ratios are presented in Fig. 7. The T_{CH} and $T_{1\rho}(H)$ measurements were obtained by fitting the CP signal intensities with the following formula [46].

$$M(t) = M_0 \exp(-t/T_{1\rho}(H))(1 - \exp(-t/T_{CH})) \quad (4)$$

where $M(t)$ is the peak intensity as a function of contact time t, M_0 is the normalization constant, $T_{1\rho}(H)$ is the proton spin-lattice relaxation in the rotating frame, and T_{CH} is the cross-polarization time constant. Since the CP efficiency depends on the magnetization transfer by the dipolar coupling from ^1H to ^{13}C, the CP process is most efficient for the static ^1H–^{13}C dipolar interactions. Therefore, the less mobile carbon groups exhibit the faster cross-polarization rate or the shorter T_{CH}. The $-OCH_2$ groups (71 ppm) exhibit T_{CH} values of 0.88 and 0.29 ms and $T_{1\rho}(H)$ values of 32.4 and 14.8 ms for the C(600)–Z hybrids with [O]/[Li] ratio of 32 and 8, respectively. The slower growth in spin magnetization for the peak at 71 ppm for C(600)–32 reflects that the rapid motion of the polymer chains makes the CP signal transfer from the proton spins less efficient as compared to the case of C(600)–8. The significant decrease in T_{CH} for the peak at 71 ppm with increasing salt concentrations also suggests a possible coordination of Li^+ ions with the ether oxygen atoms of the polymer chain, thereby restricting the segmental motion of the polymer chains.

3.7. 2D ^1H–^{13}C WISE NMR

2D WISE NMR has been widely used for determining dynamic heterogeneities in solid polymers [17]. By means of 2D WISE NMR, the spectroscopic information about the dynamic behavior within a polymer system can be qualitatively assessed by examining the proton line shapes that are directly related to structural elements resolved in the ^{13}C CPMAS NMR spectrum. The line width of the ^1H line in the second dimension reflects the nature of the dipolar interaction between the proton spins and thus can be used to monitor the segmental mobility of the polymer chains. Fig. 8 shows the representative 2D ^1H–^{13}C WISE spectrum and the projections of the ^1H dimension associated with the 71 ppm peak in the ^{13}C dimension for C(600)-Z hybrids with [O]/[Li] ratios of 32 and 8 (parts b and c in Fig. 8). The line width of the ^1H line reflects the nature of the dipolar interaction between the protons and thus can be used to monitor the mobility of polymer chains. For the selected carbon at 71 ppm, the C(600)–Z hybrids with [O]/[Li] ratio of 8 exhibited a larger line width (2.4 kHz) in the ^1H dimension than the C(600)-Z hybrids with [O]/[Li] ratio of 32 (2.1 kHz). This reflects some microscopic dynamic changes of the polymer chains as the salt concentration is increased. Thus, the 2D WISE NMR spectra further

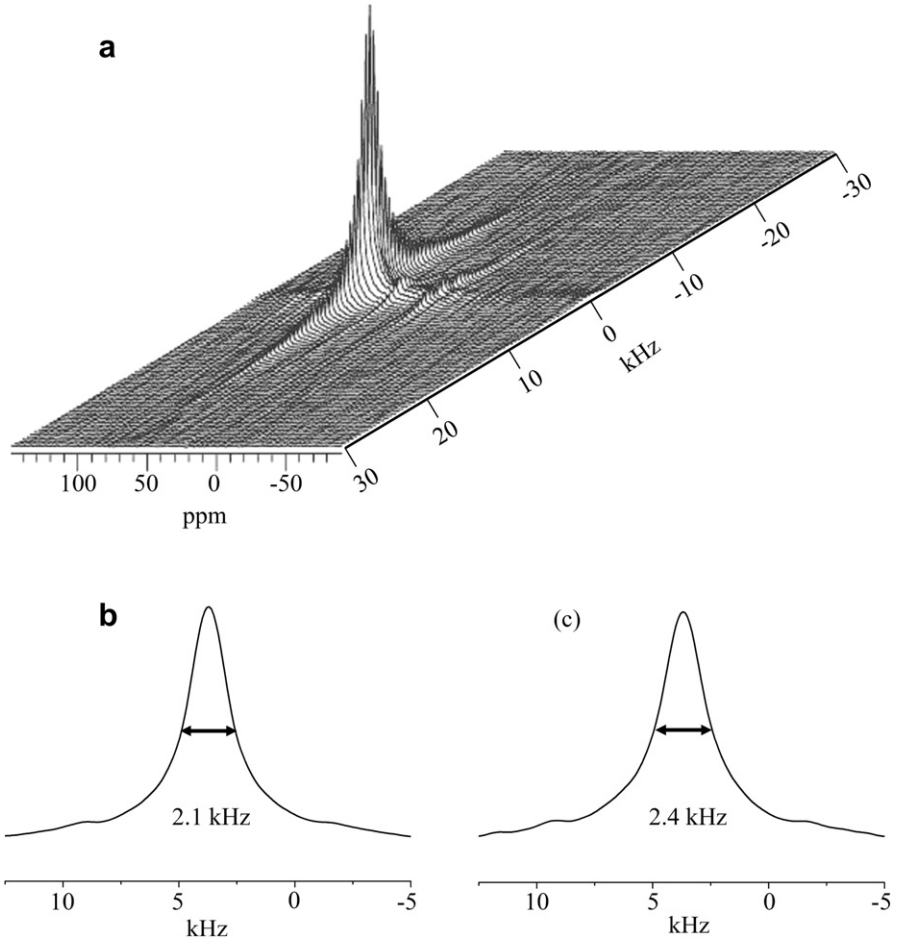

Fig. 8. (a) Representative 2D ^1H–^{13}C WISE NMR spectrum and the projection of ^1H dimension of 2D ^1H–^{13}C WISE spectra associated with the 71 ppm peak in the ^{13}C dimension for (b) C(600)–32 and (c) C(600)–8.

confirms that the mobility of the polymer chains decreases as the salt content is increased due to complexation of lithium cations with the ether oxygen atoms. While compared with the ^{1}H line width of crystalline or semicrystalline polymers (>50 kHz), the much narrower proton line width from the 2D WISE NMR reveals considerable chain mobility for the present hybrid electrolytes. A microscopic change in the mobility of the polymer chains as a function of salt concentrations can be monitored with this technique, which is often not obtainable by other characterization techniques.

3.8. ^{7}Li line width measurements

The mobility and transport of the Li-ion in a dynamic environment created by the polymer motion in the amorphous phase is a key factor for the ionic conductivity. The Li-ion mobility was investigated by measuring the line width of the central ^{7}Li transition as a function of salt concentration as well as temperature. Below the T_g, the ^{7}Li spectra consist of a very intense central transition ($1/2 \rightarrow -1/2$) and an almost unobservable weak and broad line that could be associated with the quadrupolar satellite transitions ($3/2 \rightarrow 1/2$ and $-1/2 \rightarrow -3/2$). Above the T_g, the weak and broad line associated with the quadrupolar satellite peaks is averaged out. That is, for nuclear spins $I > 1/2$ with small quadrupolar moment such as ^{7}Li, the central transition line width is primarily determined by dipole–dipole interactions [27,47,48]. For this reason, only the ^{7}Li central transition was analyzed in this study.

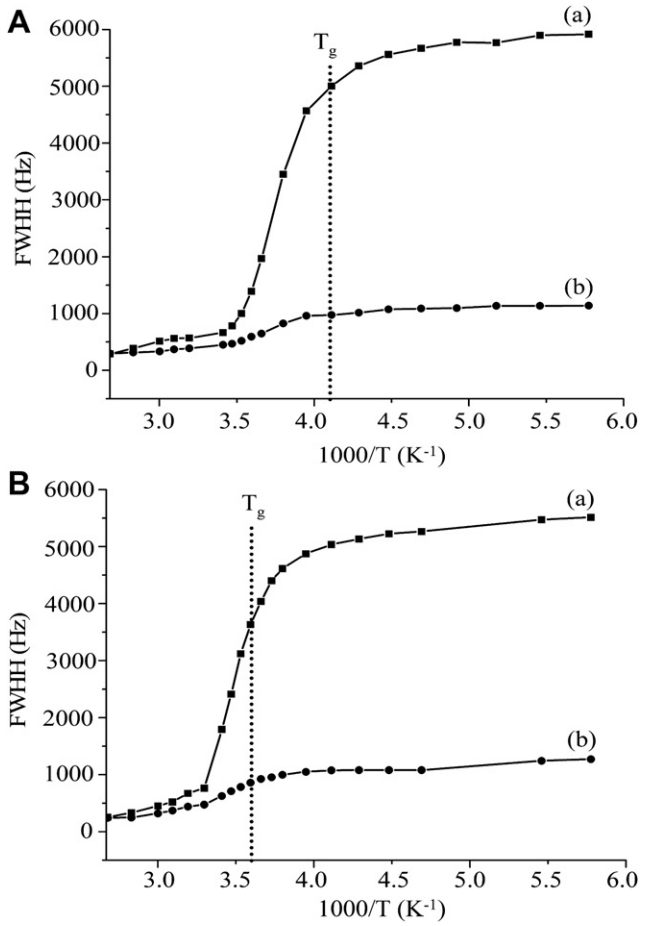

Fig. 9. Temperature dependence of ^{7}Li static line widths of C(600)–Z hybrids with [O]/[Li] ratios of (A) 32 and (B) 8 measured (a) without and (b) with proton decoupling. The dashed lines represent the T_g values obtained from DSC.

Fig. 9 displays the ^{7}Li central transition line widths as a function of temperature for the C(600)-Z hybrid electrolyte with [O]/[Li] ratios of 32 and 8, with and without proton decoupling. Below the T_g (ca. −20 °C) of the hybrid electrolyte, the line widths are very broad (FWHH = 5–6 kHz) and are approaching the rigid lattice line width. This suggests that the Li-ions are essentially immobile and therefore the line width is the result of increased quadrupolar or internuclear dipole–dipole interactions. Upon increasing the sample temperature, the line widths are slowly narrowed. The ^{7}Li line width decreases from 6.0 to 1.0 kHz in the low-temperature region (i.e., −100 to −30 °C) by the use of the proton decoupling techniques. This clearly demonstrates that the line width of ^{7}Li NMR spectra is predominately governed by ^{1}H–^{7}Li dipolar interactions (about 85% of all ^{7}Li spin interactions). As the temperature increases, the line widths are gradually narrowed, with the onset of narrowing closely related to the T_g of the hybrid electrolytes measured by DSC experiments. It should note that the T_g measured by DSC is a macroscopic property, whereas the ^{7}Li line width measured by NMR is a microscopic property. Any change in mobility will lead to the change in the ^{7}Li line width. Therefore, the ^{7}Li line width is more sensitive to the mobility change than T_g. As a result, the onset temperature of the narrowing of the ^{7}Li line width is slightly lower than the T_g value (Fig. 9). Overall, the motions of the lithium cations are strongly coupled with the segmental motion of the polymer chains, which is in very good accordance with the VTF behavior as observed in ionic conductivity. The line widths also reach the high-temperature limit due to inhomogeneities of magnetic field. On the other hand, the line width for the hybrid electrolyte with [O]/[Li] = 32 was smaller as compared to the [O]/[Li] = 8 over the temperature range investigated, suggesting its higher Li-ion mobility that correlates with its higher conductivity.

3.9. Linear sweep voltammetry

The electrochemical stability of the hybrid electrolytes was investigated by linear sweep voltammetry to endure the operating voltage of the battery system. As the ionic conductivity of the C(2000)–Z hybrid electrolyte was higher than C(900)–Z and C(600)–Z hybrids, linear sweep voltammetry studies were carried out on C

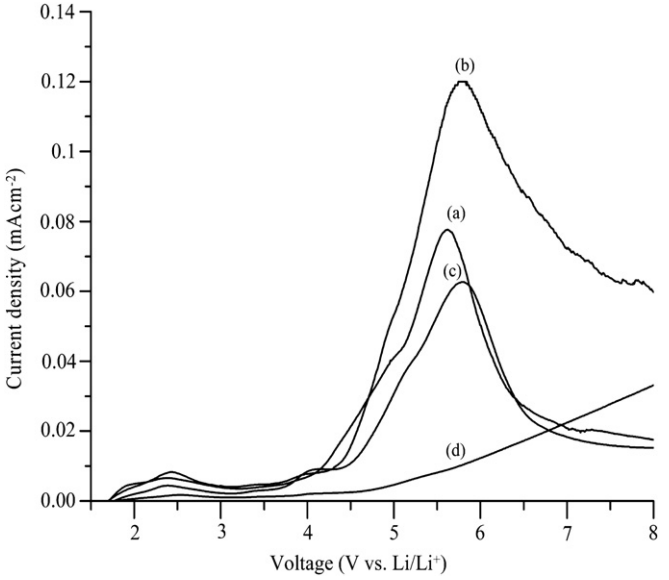

Fig. 10. Linear sweep voltammetry curves of the cell prepared with C(2000)–Z hybrid electrolyte with various [O]/[Li] ratios, Z = (a) 32, (b) 24, (c) 16 and (d) 8.

(2000)–Z series. Fig. 10 shows the linear sweep voltammogram of Li/C(2000)–Z/SS cell at a scan rate of 1 mVs^{-1} from 0 to 8 V vs. Li/Li^{+}. A very low background current was measured in the potential region between 1.5 V and above 4.0 V for the hybrid electrolyte with different [O]/[Li] ratios. A considerable current began to flow when it crossed 4.0 V, indicating the onset of electrolyte decomposition process. It is observed that electrochemical stability window slightly increases with the $LiClO_4$ concentration, from 4.0 V for [O]/[Li] = 32, 4.2 V for [O]/[Li] = 24, 4.4 V for [O]/[Li] = 16 to about 4.7 V for [O]/[Li] = 8. Therefore, it is attributed that the lithium salt also plays a role in electrochemical stability. The hump between 1.5 and 3.0 V was ascribed to the oxidation of some trace species such as water and oxygen [49]. The result shows that the electrochemical stability window of the C(2000)–Z hybrid electrolyte is above 4.0 V, which is sufficient for its possible use in lithium-ion batteries.

4. Conclusions

A hyperbranched polymer system has been synthesized as an alternative to PEO for use as a solid electrolyte for lithium batteries with varying the molecular weight of the polymer. The effect of lithium salt concentrations on conductivity, ion structure and dynamics has been investigated and found significant improvement of ionic conductivity and mechanical stability. The highest room temperature ionic conductivity is found to be 6.8×10^{-5} Scm^{-1} for the C(2000)–Z series with a [O]/[Li] ratio of 32. Specific interactions among ions and polymer matrix have been examined in detail by ^{13}C CPMAS and 2D WISE NMR experiments: both confirmed that the segmental mobility of the polymer matrix is affected by salt concentration. Lithium transference number and linear sweep voltammetry measurements revealed comparable lithium ion movements and electrochemical stability up to 4.7 V. Based on these results, it is anticipated that the present hybrid electrolytes have specific interest for the development of advanced rechargeable lithium batteries.

Acknowledgment

The financial support of this work by the National Science Council of Taiwan is gratefully acknowledged.

Appendix. Supplementary material

Supplementary data associated with article can be found in the online version at doi:10.1016/j.polymer.2010.07.039.

References

[1] MacCallum JR, Vincent CA. Polymer electrolyte reviews 1 and 2. London: Elsevier; 1987 and 1989.
[2] Gray FM. Solid polymer electrolytes. New York: VCH Publishers; 1991.
[3] Scrosati B. Application of electroactive polymers. London: Chapman & Hall; 1993.
[4] Meyer WH. Adv Mater 1998;10:439–48.
[5] Armand M. Solid State Ionics 1994;69:309–19.
[6] Druger SD, Nitzan A, Ratner MA. J Chem Phys 1983;79:3133–42.
[7] Nishimoto A, Agehara K, Furuya N, Watanabe T, Watanabe M. Macromolecules 1999;32:1541–8.
[8] Nicholas CV, Wilson DJ, Booth C, Giles JRM. Br Polym J 1988;20:289–92.
[9] Allcock HR, Kuharcik SE, Reed CS, Napierala ME. Macromolecules 1996;29:3384–9.
[10] Chen-Yang YW, Hwang JJ, Hung AY. Macromolecules 2000;33:1237–44.
[11] Croce F, Appetecchi GB, Persi L, Scrosati B. Nature 1998;394:456–8.
[12] Kumar B, Rodrigues SJ. J Electrochem Soc 2001;148:A1336–40.
[13] Liang WJ, Kuo PL. Polymer 2004;45:1617–26.
[14] Kao HM, Chao SW, Chang PC. Macromolecules 2006;39:1029–40.
[15] Tigelaar DM, Meador MAB, Kinder JD, Bennett WR. Macromolecules 2006;39:120–7.
[16] Evans J, Vincent CA, Bruce PG. Polymer 1987;28:2324–8.
[17] Schmidt-Rohr K, Clauss J, Spiess HW. Macromolecules 1992;25:3273–7.
[18] Saikia D, Wu HY, Pan YC, Liao CC, Chen CF, Fey GTK, et al. Electrochim Acta 2009;54:7156–66.
[19] Silva MM, de Zea Bermudez V, Carlos LD, de Almeida APP, Smith MJ. J Mater Chem 1999;9:1735–40.
[20] Babonneau F, Dire S, Bonhomme-Coury L, Livage J. Inorganic and organometallic polymers. ii. sol-gel synthesis of heterometallic oxo polymers. ACS Symposium Series 134. Washington, D.C: American Chemical Society; 1994 [Chapter 12].
[21] Kao HM, Hung TT, Fey GTK. Macromolecules 2007;40:8673–83.
[22] Carlos LD, de Zea Bermudez V, Sá Ferreira RA. J Non-Cryst Solids 1999;247:203–8.
[23] Miyazawa T, Shimanouchi T, Mizushima SI. J Chem Phys 1956;24:408–18.
[24] Papke BL, Ratner MA, Shriver DF. J Phys Chem Solids 1981;42:493–500.
[25] Eschmann J, Strasser J, Xu M, Okamoto Y, Eyring EM, Petrucci SJ. Phys Chem 1990;94:3908–16.
[26] Kioul A, Mascia LJ. Non-Cryst Solids 1994;175:169–86.
[27] Mello NC, Bonagamba TJ, Panepucci H, Dahmouche K, Judeinstein P, Aegerter MA. Macromolecules 2000;33:1280–8.
[28] Dahmouche K, Atik M, Mello NC, Bonagamba TJ, Panepucci H, Aegerter M, et al. Sol-Gel Sci Technol 1997;8:711–5.
[29] de Souza PH, Bianchi RF, Dahmouche K, Judeinstein P, Faria RM, Bonagamba TJ. Chem Mater 2001;13:3685–92.
[30] Zhang J, Huang X, Wei H, Fu J, Huang Y, Tang X. Electrochim Acta 2010;55:5966–74.
[31] Jeyapandian M, Lavina S, Thayumanasundaram S, Ohno H, Negro E, Noto VD. J Power Sources 2010;195:341–53.
[32] Barbosa PC, Silva MM, Smith MJ, Gonçalves A, Fortunato E, Nunes SC, et al. Electrochim Acta 2009;54:1002–9.
[33] Souza FL, Bueno PR, Longo E, Leite ER. Solid State Ionics 2004;166:83–8.
[34] Qi L, Dong SJ. Chin Chem Lett 2007;18:185–8.
[35] Higa M, Yaguchi K, Kitani R. Electrochim Acta 2010;55:1380–4.
[36] Wang L, Li X, Yang W. Electrochim Acta 2010;55:1895–9.
[37] Derrien G, Hassoun J, Sacchetti S, Panero S. Solid State Ionics 2009;180:1267–71.
[38] Marzantowicz M, Dygas JR, Krok F, Tomaszewska A, Florjańczyk Z, Zygadło-Monikowska E, et al. Power Sources 2009;194:51–7.
[39] Souquet JL, Duclot M, Levy M. Solid State Ionics 1996;85:149–57.
[40] Samir MASA, Alloin F, Sanchez JY, Dufresne A. Macromolecules 2004;37:4839–44.
[41] Binesh N, Bhat SV. J Polym Sci B Polym Phys 1998;36:1201–9.
[42] Carvalho LM, Guégan P, Cheradame H, Gomes AS. Eur Polym J 2000;36:401–9.
[43] Liang YH, Wang CC, Chen CY. Eur Polym J 2008;44:2376–84.
[44] Cohen MH, Turnbull DJ. Chem Phys 1959;31:1164–9.
[45] Edman L, Doeff MM, Ferry A, Kerr J, De Jonghe LC. J Phys Chem B 2000;104:3476–80.
[46] Mehring M. Principles of high-resolution NMR in solids. 2nd ed. New York: Springer-Verlag; 1983.
[47] Chung SH, Jeffrey KR, Stevens JRJ. Chem Phys 1991;94:1803–11.
[48] Lin CL, Kao HM, Wu RR, Kuo PL. Macromolecules 2002;35:3083–96.
[49] Jiang YX, Chen ZF, Zhuang QC, Xu JM, Dong QF, Huang L, et al. J Power Sources 2006;160:1320–8.